A new bidirectional deconvolution method that overcomes the minimum phase assumption

Yang Zhang and Jon Claerbout

ABSTRACT

Traditionally blind deconvolution makes the assumption that the reflectivity spike series is white. Earlier we dropped that assumption and adopted the assumption that the output spike series is sparse under a hyperbolic penalty function. This approach now here allows us to take a step further and drop the assumption of minimum phase. In this new method (what we called Bidirectional Sparse Deconvolution), We solve explicitly for the maximum phase part of the source. Results on both synthetic data and field data show clear improvements.

INTRODUCTION

In the previous report (Zhang and Claerbout, 2010), we introduced the spiking deconvolution problem using the hybrid norm solver (Claerbout, 2009a). Synthetic examples (Zhang and Claerbout, 2010) showed that given a minimum-phase wavelet, it retrieved the sparse reflectivity model almost perfectly even with a reflection series that is far from white, while conventional L2 deconvolution did a poor job. However, if the assumption of a minimum-phase wavelet was removed, the hybrid norm spiking deconvolution failed quickly and gave a poor result similar to the conventional L2 deconvolution.

In this paper, we still rely on the hybrid norm solver to retrieve the sparse model, but we use a slightly more complex formulation that avoids the minimum-phase wavelet constraint.

We start by realizing that any (mixed-phase) wavelet $C(Z)$ can be decomposed into a minimum-phase part $A(Z)$ and a maximum-phase part $B(1/Z)$ plus a certain time shift:

$$C(Z) = A(Z)B(1/Z)Z^k, \tag{1}$$

where $B(Z)$ is also a minimum-phase wavelet (therefore $B(1/Z)Z^k$ is a maximum-phase wavelet) and the exponent k is the order of $B(Z)$. This Z^k term makes the wavelet $C(Z)$ causal. In the time domain, (1) can be written as

$$c = a * b^r * \delta(n-k), \tag{2}$$

where b^r stands for the time reverse of series b.

Our original spiking deconvolution can find only a minimum-phase wavelet which has the same spectrum of real wavelet c. It can be defined as an inverse problem as follows:

$$[d]f_c = r, \tag{3}$$

where $[d]$ is the data convolution operator, and f_c is the unknown filter. In this formulation, the filter is the only unknown, the hybrid norm is applied on the residual term r to enforce the sparseness constraint. In theory, the residual r itself is the reflectivity model. Such a method requires the wavelet in the data to be minimum-phase because only a minimum-phase wavelet has a causal stable inverse.

The following bidirectional deconvolution formulation utilizes a pair of conventional deconvolutions, trying to invert components a and b separately:

$$\begin{array}{l} [(d * f_b^r)]\, f_a = r_a, \\ [(d * f_a)^r]\, f_b = r_b, \end{array} \tag{4}$$

in which f_a and f_b are the corresponding filters that corresponds to the inverses of a and b denoted above, the superscript r means time-reverse. The operator in each equation is the convolution operator. Again the hybrid norm is applied to r_a and r_b, and the reflectivity model is simply r_a plus a time shift. Notice that this is a non-linear inversion, since the operator itself depends on the unknown f_a and f_b. In practice we have to solve these two inversions alternately and therefore iteratively.

To understand the meaning of (4), let

$$d = m * c = m * a * b^r * \delta(n-k), \tag{5}$$

where m is the reflectivity model and the δ term is just a time shift. Assume f_a and f_b are perfectly known in the operators (which is not true in reality), i.e.

$$f_a * a = \delta(n), f_b * b = \delta(n)$$

Substituting (5) into (4), since

$$d * f_b^r = m * \delta(n-k) * a, \tag{6}$$

$$(d * f_a)^r = (m * b^r * \delta(n-k))^r = m^r * \delta(n+k) * b, \tag{7}$$

we have

$$\begin{array}{l} [(m * \delta(n-k)) * a]\, f_a = r_a, \\ [(m^r * \delta(n+k)) * b]\, f_b = r_b. \end{array} \tag{8}$$

From (8) it is easier to see what is behind the bidirectional deconvolution formulation (4): It tries to separate the two parts of the wavelet, turning each one into a traditional deconvolution problem in which the wavelet (a, b) is always minimum-phase.

As with all non-linear estimation, iteration is required. Convergence is assured if the starting solution is close enough. We expect the traditional PEF for a and an impulse function for b to be a pretty good first guess. The following section shows several examples (complexity varies from low to high) illustrating the effectiveness and limitations of the method.

DATA EXAMPLES

Inverting a single wavelet

To verify the bidirectional deconvolution's ability to handle mixed-phase wavelets, we first set the input data to be a single wavelet, to see whether the data can be compressed to a single spike. We choose three types of wavelets as inputs:

1. a minimum-phase wavelet used in the previous report (Zhang and Claerbout, 2010), referred to as wavelet 1.
2. a wavelet that deviates slightly from minimum-phase: it models a simple marine ghost – a low frequency function passing through a time derivative at the source and another at the receiver. The low frequency function chosen is the convolution of two one-sided triangles.
3. a zero-phase wavelet created by convolving the minimum-phase with its own time-reverse wavelet. Such wavelet has identical a and b components, referred to as wavelet 3.

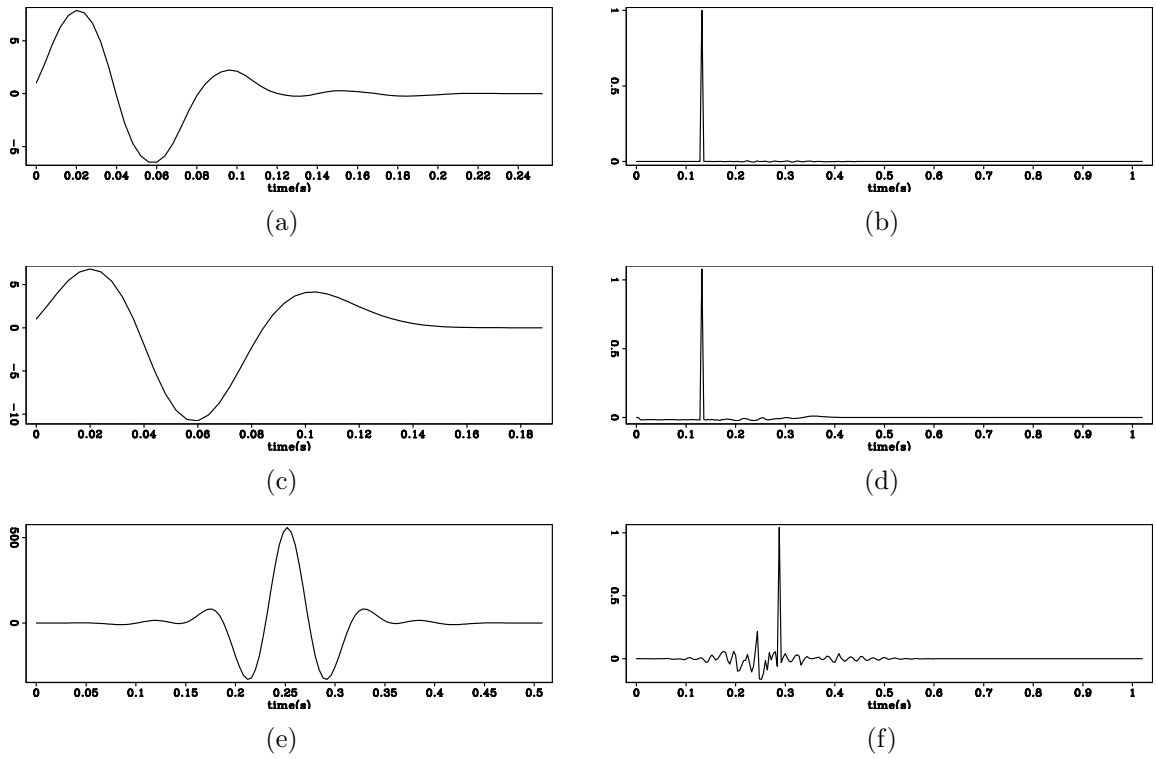

Figure 1: (a) Input wavelet 1 and (b) its deconvolution result. (c) Input wavelet 2 and (b) its deconvolution result. (e) Input wavelet 3 and (f) its deconvolution result. [**ER**]

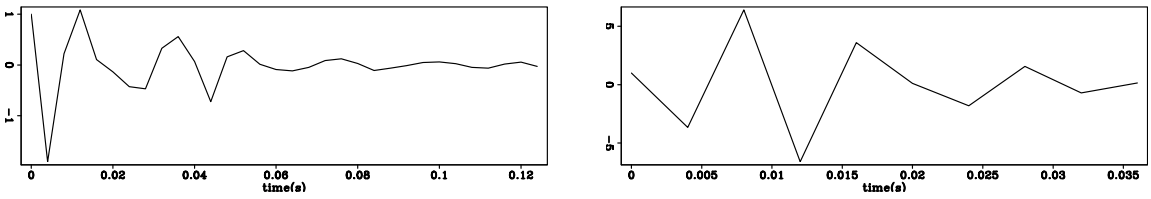

(a) (b)

Figure 2: For the wavelet 3 inversion, (a) filter f_a; (b) filter f_b. [**ER**]

Figure 1(a) 1(b), figure 1(c) 1(d) and figure 1(e) 1(f) show wavelets 1,2,3, and the results of reflectivity models respectively. In all 3 cases, our bidirectional deconvolution method is able to compress the wavelet into a spike.

Figure 2 shows the retrieved filters f_a and f_b from wavelet 3's inversion. Notice that f_a and f_b given by the inversion are different from each other, while ideally they should be the same, since a and b are the same when we create wavelet 3. This observation indicates that the solutions f_a and f_b of this method do not necessarily converge to the inverse of the initial a and b.

Inverting a synthetic trace

Next we try a more complex example where the data is generated by convolving each type of wavelet with a sparse reflectivity series. Figure 3 shows the reflectivity series.

Figure 4(a) 4(b), figure 4(c) 4(d) and figure 4(e) 4(f) show the data created using wavelets 1,2,3, and the recovered reflectivity models respectively. In all 3 cases, the reflectivity model is well recovered; however the polarity of the reflectivity model from wavelet 3 case is opposite to that of the real reflectivity model; this unexpected change of polarity shows the uncertainty of the convergence point in our non-linear formulation. We think this polarity change is not an issue in our blind deconvolution scenario.

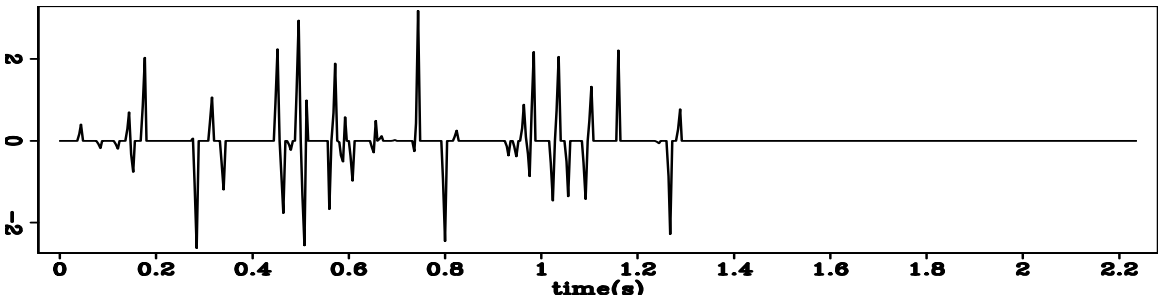

Figure 3: reflectivity model trace. [**ER**]

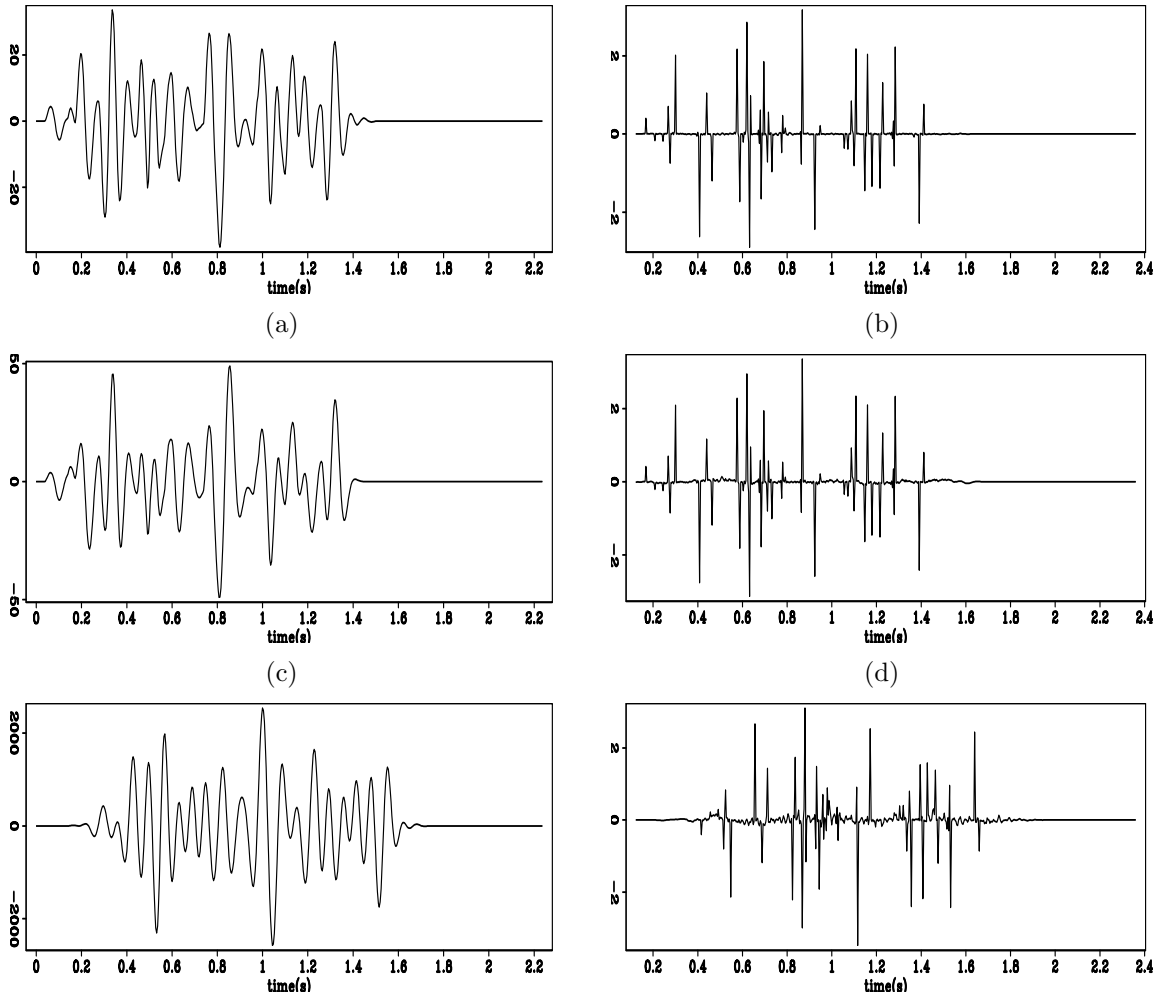

Figure 4: (a) The data trace generated using wavelet 1; (b) the recovered reflectivity model of (a). (c) The data trace generated using wavelet 2; (d) the recovered reflectivity model of (c). (e) The data trace generated using wavelet 3; (f) the recovered reflectivity model of (e). [**ER**]

Inverting a 2D synthetic section

As in the previous report (Zhang and Claerbout, 2010), we use a 2D synthetic reflectivity model from Claerbout (2009b). Figure 5(a) shows the starting reflectivity model. Figure 5(b) shows the data generated by convolving the reflectivity model with wavelet 3. All traces use the same wavelet when generating the data, and all traces share the same wavelet when we are doing the deconvolution.

Previously the traditional sparse deconvolution failed on this example because of the symmetric wavelet; therefore, here we compare the old method and the bidirectional deconvolution method. Figure 6(a) shows the result using the old method (equation (3)). Figure 6(b) shows the result using the bidirectional deconvolution method (equation (4)). Comparing to the given model, the bidirectional deconvolution result is a spectacular improvement over the old one. Bidirectional deconvolution is a big improvement.

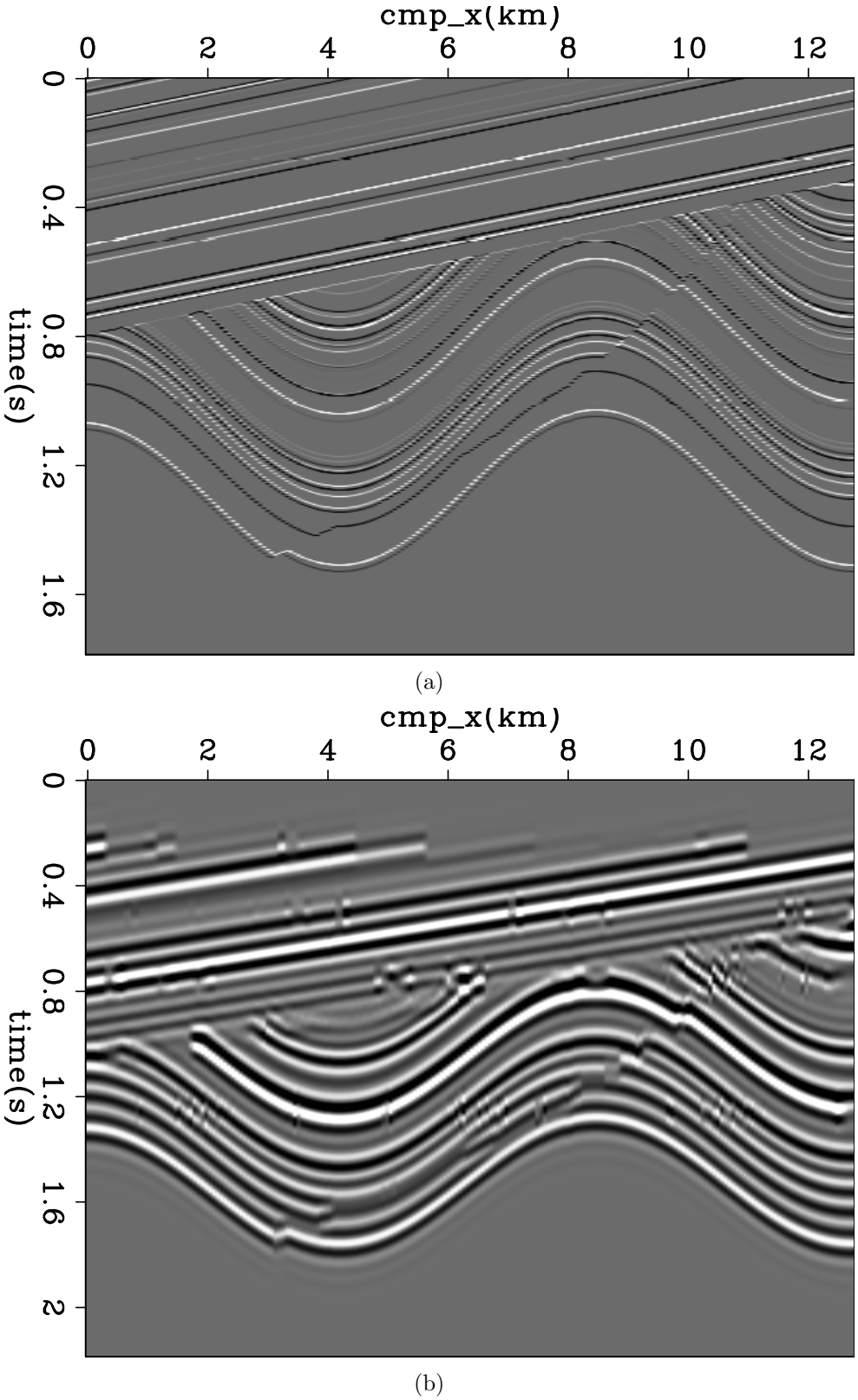

(a)

(b)

Figure 5: (a) The 2D synthetic reflectivity model; (b) the synthetic data generated using wavelet 3. [**ER**]

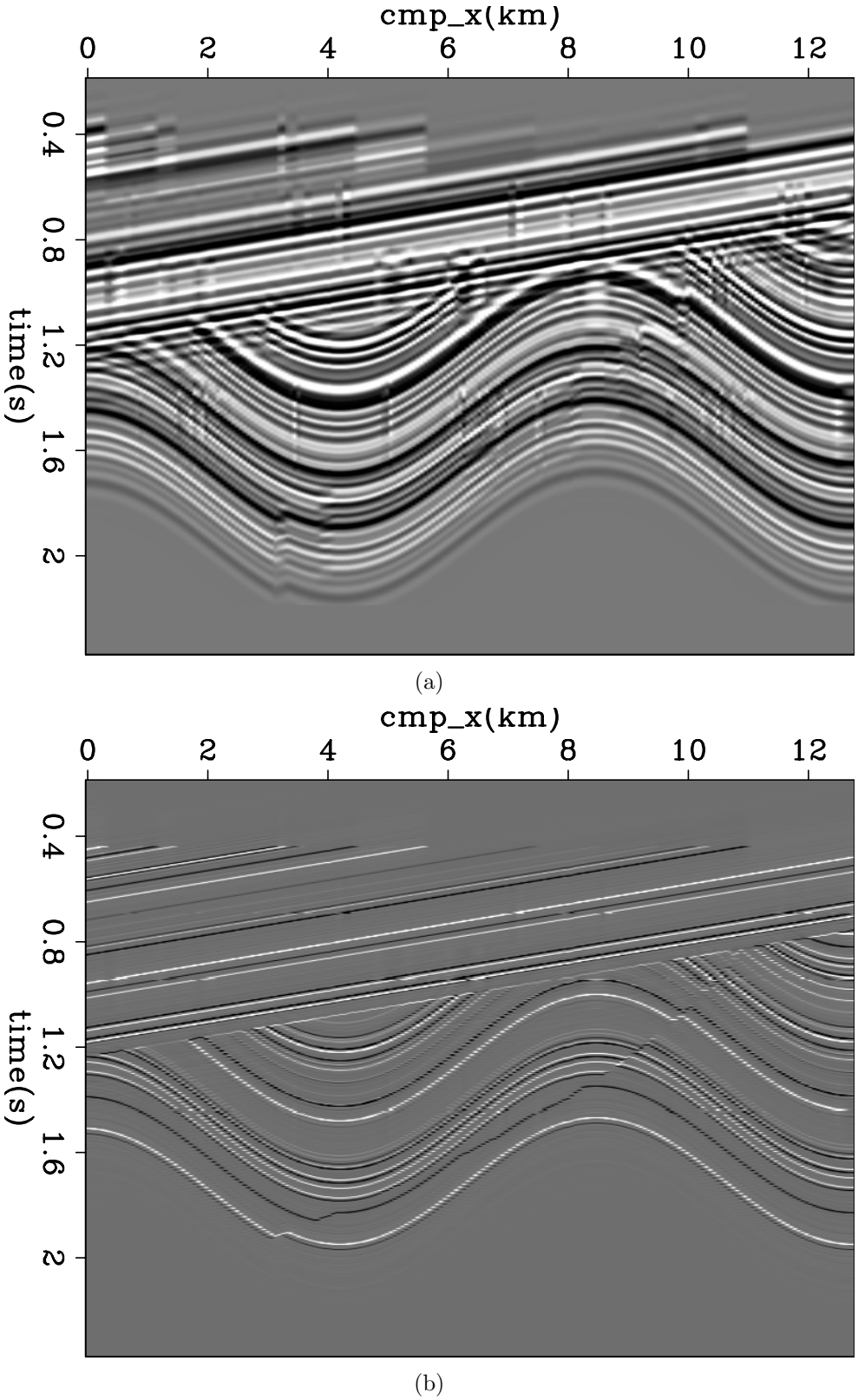

Figure 6: (a) reflectivity model retrieved from the original method; (b) reflectivity model retrieved from the bidirectional deconvolution method. [**ER**]

Inverting a 2D field section

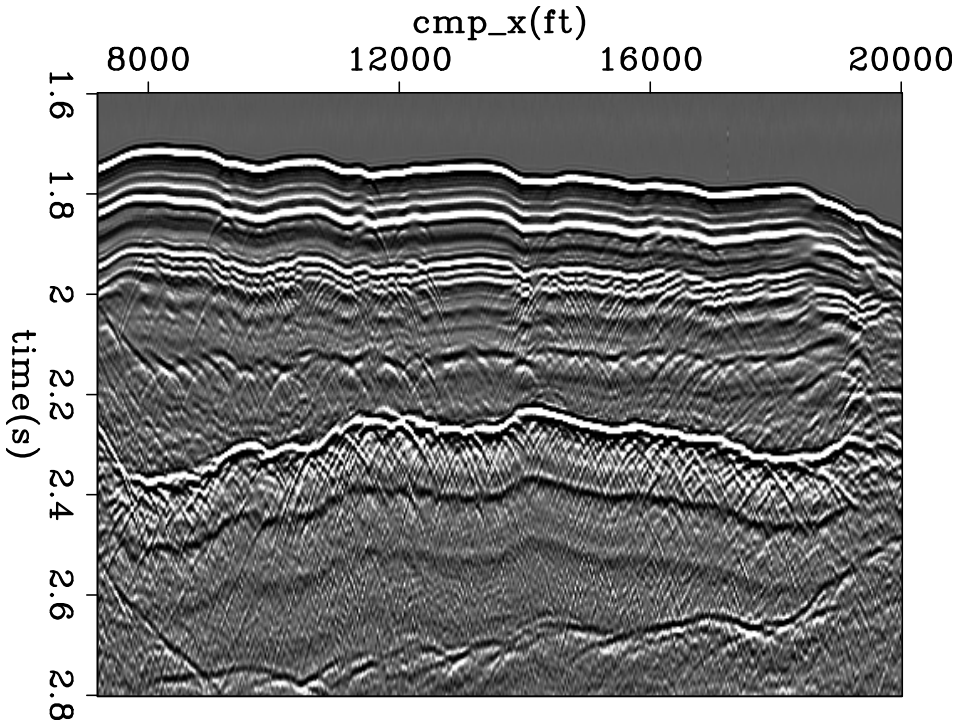

Figure 7: Input Common Offset data. [**ER**]

The second example is a common-offset section of marine field data. Figure 7 shows the input data. Figure 8(a) shows the result using the old method. Figure 8(b) shows the result using the bidirectional deconvolution method.

The raw data in Figure 7 shows strong events like a double ghost (black, white, black). The traditional PEF result in Figure 8(a) shows strong events like doublets (black, white). The bidirectional deconvolution result in Figure 8(b) shows strong events like singlets (white). Examining Figure 8(b) we notice events at about 1.85s (black), 1.95s (black), 2.3s (white), 2.4s(black), 2.5s (mixed), and 2.8s (white). The unipolarity of individual suggests that a causal integration would produce the step functions we associate with impedence in a blocky model. Figure 9 is a first attempt to compute the impedence from the reflectivity in Figure 8(b). This was done by causal integration and some horizontal smoothing. Ideally, Figure 8(b) has only isolated white events and black events defining geologic boundaries. Time integrating these impulsive events should yield positive rectangle functions. Actually, the result we see in Figure 9 looks more like leaky integration of Figure 8(b). The small events present in Figure 8(b) apparently contains low frequency energy at the opposite polarity of that of the isolated impulses. We could thus regard Figure 9 as a failure. Instead we regard it as an inverse problem that we have not yet correctly posed. The failure arises because the raw data fails to contain the required low frequencies. Were we to replace small values in Figure 8(b) by zeros, we might have obtained a result more to our liking. We need to formalize the inverse problem and reduce it to the usual situation

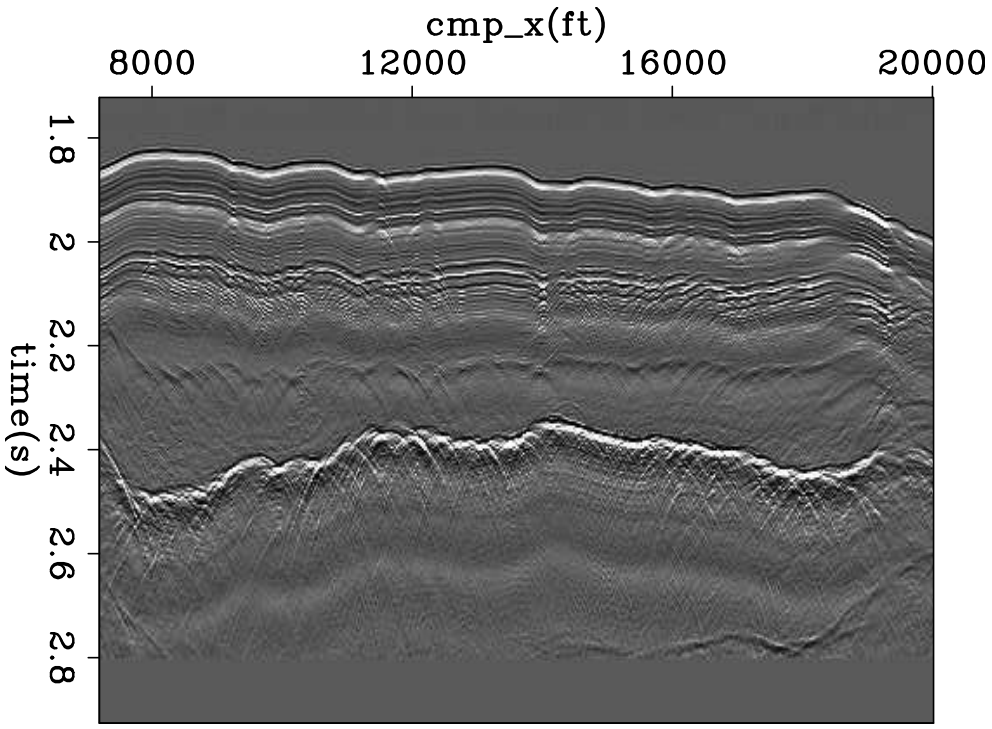

(a)

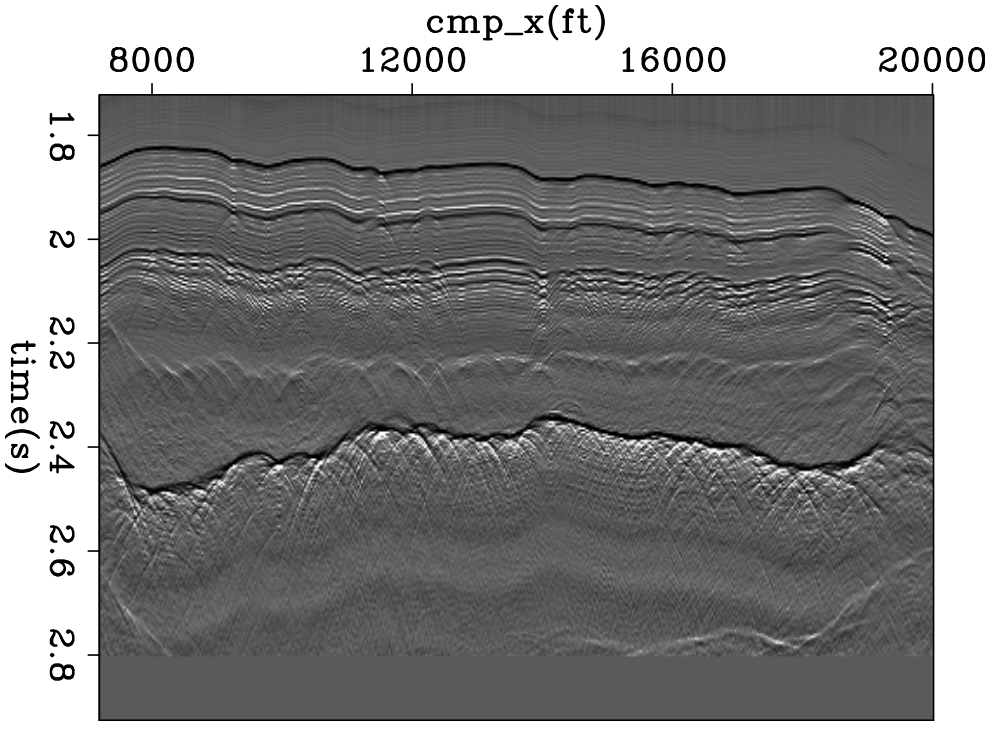

(b)

Figure 8: Given the common offset data in Figure 7, (a): reflectivity model retrieved from the original method; (b): reflectivity model retrieved from the bidirectional deconvolution method. [**ER**]

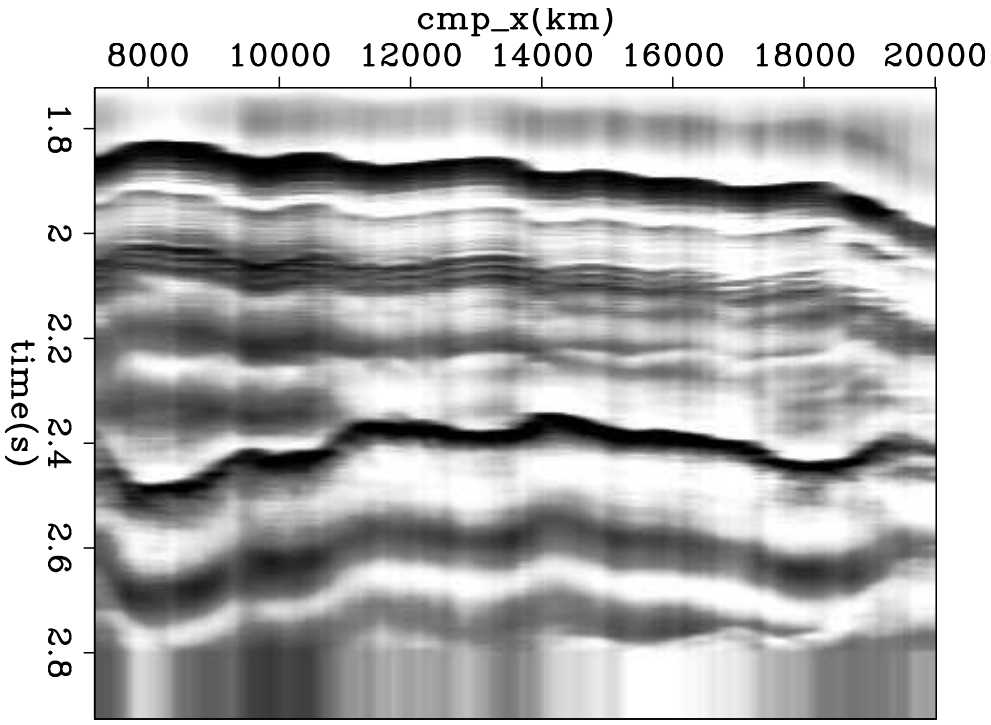

Figure 9: Causal time integration of the reflectivity in figure 8(b). This should be the impedence. [**ER**]

which is how much to regard the data as perfect, and how to allow imperfection to be overcome by methodology that tends us to blocky models.

CONCLUSION

We demonstrate what we anticipated theoretically that we can overcome the minimum phase assumption in blind deconvolution. Our process is non-linear, but (we claim) not extremely so. To be successful it does require a non-Gaussian distribution of impulses. Likewise, the iteration has a few adjustable parameters which makes its use a little more difficult, but we do not anticipate serious difficulties in practice. One interesting phenomenon about the bidirectional deconvolution (Figure 1(e) 1(f) and figure 2) is that it was able to compress a mixed-phase wavelet to a spike but without obtaining the correct causal and anti-causal parts. We do not yet understand this. In addition, it is more costly because it requires multiple iterations.

FUTURE WORK

Having had good fortune here introducing the anti-causal PEF and earlier explicitly estimating a portion of the data not fitting the convolutional model (Zhang and

Claerbout, 2010) , it is natural to try introducing both at the same time. That takes into account the fact that a part of the input data does not fit the convolution model:

$$\left\{ \begin{bmatrix} (d * f_b^r) & -\mathbf{I} \\ \mathbf{0} & \epsilon\mathbf{I} \end{bmatrix} \begin{bmatrix} f_a \\ m_a \end{bmatrix} \approx \begin{bmatrix} r_{da} \\ r_{ma} \end{bmatrix}, \tag{9}$$

$$\left\{ \begin{bmatrix} (d * f_a)^r & -\mathbf{I} \\ \mathbf{0} & \epsilon\mathbf{I} \end{bmatrix} \begin{bmatrix} f_b \\ m_b \end{bmatrix} \approx \begin{bmatrix} r_{db} \\ r_{mb} \end{bmatrix}, \tag{10}$$

in both matrices on the upper left is the data convolution operator, f_a and f_b are the filters, and m_a and m_b are the reflectivity models. The parameter ϵ indicates the strength of the regularization. We apply the hybrid norm on model residuals r_{ma} and r_{mb} to enforce sparseness. Although the extra parameter tuning (ϵ) is undesirable, we expect to get more successful result using this more advanced formulation.

ACKNOWLEDGMENTS

The authors thank the sponsors of Stanford Exploration Project for the financial support, and also thank Bob Clapp, Antoine Guitton and Luis Canales for fruitful discussions.

REFERENCES

Claerbout, J., 2009a, Blocky models via the l1/l2 hybrid norm: SEP-Report, **139**, 1–10.

Claerbout, J. F., 2009b, Basic earth imaging.

Zhang, Y. and J. Claerbout, 2010, Least-squares imaging and deconvolution using the hb norm conjugate-direction solver: SEP-Report, **140**, 129–142.